Microscale Strain Partitioning? Differential Quartz Crystallographic Fabric Development in Phyllite, Hindu Kush, Northwestern Pakistan

Kyle P. Larson[1*], Jaida L. Lamming[2,1], Shah Faisal[1]

[1]*Earth and Environmental Sciences, University of British Columbia, Okanagan, 3247 University Way, Kelowna, BC, V1V 1V7, Canada*

[2]*Department of Geological Sciences, University of Saskatchewan, 114 Science Place, Saskatoon, SK, S7N 5E2, Canada*

[*]Corresponding author - kyle.larson@ubc.ca

Abstract

Spatially referenced quartz *c*-axis fabrics demonstrate the preservation of multiple, distinct fabrics in a specimen collected from northwestern Pakistan. The overall fabric yielded by the specimen is dominated by a single population of quartz grains, while the fabric signatures of two other unique, spatially distinct populations are overwhelmed. It is these minor fabrics, however, that provide information on temperature of deformation (403± 50 ˚C), differential stress (8.6 + 2.6/-1.5 MPa to 15.0 +3.8/-2.5 MPa), strain rate (10^{-16} s^{-1} to 10^{-15} s^{-1}), and strain partitioning recorded by the specimen.

1. Introduction

Crystallographic analysis has been long employed to study the strain histories recorded by rock forming minerals (e.g. Turner, 1942; Sander, 1950; Bouchez and Pêcher, 1976; Zhang and Karato, 1995). While investigation of crystallographic fabrics have been successfully carried out on a wide variety of mineral phases, quartz has been one of the most common targets to

elucidate strain within continental crust due to its near ubiquity in such rocks. The development of crystallographic fabrics in quartz has been actively investigated (e.g Lister and Williams, 1979; Schmid and Casey, 1986) and utilized in studies of geologic material (e.g. Bouchez and Pêcher, 1976; Blumenfeld et al., 1986; Law et al., 1990, 2004, 2011, 2013; Xypolias and Koukouvelas, 2001; Larson and Cottle, 2014) during the past five decades. While advances in our understanding and implications of the fabrics have advanced, so too have the methods available to extract lattice orientation data. Universal stages are still employed to generate quartz *c*-axis crystallographic fabrics (e.g. Kile, 2009), however, more technical methods such as x-ray goniometry (e.g. Wenk, 1985) and electron backscattered diffraction (EBSD) (e.g. Prior et al., 1999) can potentially provide a higher density of information and orientation data for secondary axes. In addition, techniques utilizing EBSD and automated optical fabric analysers (e.g. Wilson et al., 2003; 2007) have the advantage of producing spatially referenced data with the ability to automatically generate achsenverteilungsanalyse (AVA) or axial distribution diagrams (e.g. Sander, 1950). Such a diagram, essentially a map of crystallographic orientation within the specimen analysed, can help facilitate the investigation and comparison of spatially distinct grains, groups of grains, or zones within a specimen. Spatially referenced crystallographic fabrics also allow for the investigation of strain recorded in grains of various sizes, the potential effects of matrix phases, and the spatial positioning of grains adjacent to local features such as porphyroclasts.

One significant application of spatially referenced crystallographic fabric data is to examine within-specimen fabric orientation heterogeneities. This type of analysis has been employed to distinguish between preferred orientations in new, recrystallized grains vs. relict porphyroclasts (e.g. Law et al., 2010) and to identify variable dissolution in quartz veins (Wilson

et al., 2009). Such studies highlight the potentially significant differences in LPOs for distinct grain populations and/or spatially separated areas of a single specimen.

This study presents new, spatially referenced crystallographic fabric data from a specimen collected in the Chitral region of northwestern Pakistan. This specimen records three distinct quartz crystallographic fabrics that can be related to differences in spatial position, recrystallized grain size, and interaction with matrix phases in the specimen. The existence of different crystallographic fabrics that can be related to significant changes in the texture and/or mineralogy of spatially restricted areas of a specimen may provide insight into strain partitioning at the microstructural scale. Moreover, the existence of distinct crystallographic fabrics at the thin section scale has implications for the representation of strain for a specimen using a single fabric and potentially for assessing relative differences between spatially separated specimens.

2. Geological Setting

The Chitral region is located within the eastern Hindu Kush of northwestern Pakistan (Fig. 1). The geology of the area is dominated by Paleozoic protoliths, mainly low-grade metasedimentary rocks that locally reach sillimanite grade (Gaetani et al., 1996; Zanchi et al., 2000; Hildebrand et al., 2001; Zanchi and Gaetani, 2011; Faisal et al., 2014). These metasedimentary rocks are intruded by a series of plutonic bodies that range in age from Paleozoic (Kafiristan - 483 ± 21 Ma; Debon et al., 1987), through Mesozoic (Tirich Mir: 114 to 121 Ma, Desio, 1964; Hildebrand et al., 2000; Heuberger et al., 2007), to Cenozoic (Garam Chasma - 24 Ma; Hildebrand et al., 1998). The region records a protracted deformational history with earliest records indicating Late Triassic deformation and metamorphism and recent events culminating in the Early Miocene (Faisal et al., 2014).

Specimen S32, the subject of the present study, is part of a suite of quartz-rich specimens

collected in the Chitral region. It is a quartz + muscovite + chlorite phyllite (Fig. 2a, b). The foliation in the specimen is defined by planar muscovite and chlorite laths while the lineation is defined by a grain-shape fabric of the same minerals. A thin section of specimen S32 was cut parallel to the macroscopic lineation (25˚→006˚) and perpendicular to the foliation (330˚/38˚NE). The specimen has a heterogeneous mineral distribution with localized quartz-rich lenses (Fig. 2a, b) that have a bimodal grain size distribution (Fig. 2d). The coarser grain population within the lens has a median area (as calculated for an ellipse using the long and short axes of each grain) in this section of 161 μm^2 with a standard deviation of 45 and an aspect ratio of 2.5 (standard deviation of 1.0). The smaller grain size population within the quartz-rich lens is characterized by a median area of 81 μm^2 with a standard deviation of 20 and an aspect ratio of 2.3 (standard deviation of 1.0). The long axes of both grain-size populations are typically at low angles relative to the dominant foliation. The quartz-rich lenses are surrounded by phyllosilicate-rich layers that contain quartz grains with a median elliptical equivalent surface area of 52 μm^2 with a standard deviation of 13 and an aspect ratio of 2.0 (standard deviation of 0.7). These grains are typically elongate parallel to the foliation direction. The crystallographic fabrics of each quartz grain population are investigated below.

3. Methods

The specimen was oriented during collection and cut parallel to macroscopic lineation and perpendicular to the macroscopic foliation. The orientations of *c*-axes within the specimen were determined using a G50 Automated Fabric Analyser (e.g. Wilson and Peternell, 2011) with an RGB filtered, colour CCD sensor and white LEDs at an optical resolution of 10 μm. Previous research has shown that *c*-axis orientations determined using an automated fabric analyser like the G50 are indistinguishable from those determined using X-ray (Wilson et al., 2007) and

EBSD methods (Peternell et al., 2010). The G50 outputs an interactive AVA diagram (Fig. 2c), or *c*-axis map, of the thin section that was used to build crystallographic fabrics. Because each pixel of the AVA diagram has unique *c*-axis orientation data associated with it, the crystallographic fabrics of spatially distinct sections within the specimens can be investigated by picking the exact locations within grains from which the orientation data are to be extracted.

The existence of three spatially and texturally distinct quartz grain-size populations within the specimen allows the direct investigation of potential microscale quartz crystallographic fabric and strain differences. Such investigations allow assessment of the sense of shear recorded by the different populations and the slip systems active during fabric formation. Moreover, the different grain-size populations lend themselves to paleopiezometric investigation through the application of the Stipp and Tullis (2003) paleopiezometer as modified by Holyoke and Kronenberg (2010). These paleopiezometric estimates, in turn, can be combined with derived deformation temperatures to estimate strain rates. The results from this study have bearing on microscale strain, stress, and strain rate partitioning during deformation and on the potential homogenizing effects of dominant grain size populations in crystallographic fabric data, which may obscure contributions from other smaller populations.

4. Quartz Microstructures

In the equal area stereonets used to present the *c*-axis data the lineation lies horizontally across the equator while the foliation is a vertical plane cutting through the equator. The stereonets are oriented such that a dextral asymmetry indicates top-to-the east-southeast shear.

4.1 Quartz Microstructures

The quartz grains that comprise the finer and coarser populations within the quartz-rich

lens in the specimen demonstrate textural characteristics consistent with dynamic recrystallization. In both populations there is evidence of minor bulging (Fig. 3a), subgrain development (Fig. 3b, c), and deformation lamellae (Fig. 3b, c). These textures are most consistent with Regime 2 crystallization of Hirth and Tullis (1992) or the SGR category of Stipp et al. (2002).

In contrast, strong evidence for dynamic recrystallization was not observed in the quartz grains found within the phyllitic matrix outside of the quartz-rich lens. Here, the grains are commonly partially surrounded by muscovite and/or chlorite laths (Fig. 3d) and as such typically have restricted contact with one another.

4.2 Quartz Crystallographic Fabric Results

When examined in bulk (i.e. looking at fabric automatically generated from a non-discriminant sampling grid) specimen S32 yields a crystallographic fabric consistent with activation of the basal <a>, prism <a>, and prism [c] slip systems (Schmid and Casey, 1986; Fig. 4a). There is a slight asymmetry in the basal <a> fabric that is consistent with top-to-the east-southeast shear. If the crystallographic fabrics of the three different sized quartz grain populations are examined individually, however, it becomes apparent that the overall, or bulk crystallographic fabric is dominated by the matrix quartz population.

The crystallographic fabric yielded from the matrix quartz bears a strong resemblance to the bulk fabric (Fig. 4b). While showing similar activation of the prism <a> and prism [c] slip systems, the matrix quartz *c*-axis fabric indicates preferred activation of the rhomb <a> slip system over basal <a>. Moreover, in the hand-picked pattern there appears to be a stronger prism <a> component and a more well-defined rhomb <a> asymmetry (top-to-the-east-southeast). The prism [c] positions also appear to define an asymmetry, but it yields the opposite shear sense to

144 that indicated by the basal <a> fabric (Fig. 4b).

145 In contrast to both the bulk and the matrix grain-size population, the fabric yielded by the
146 finer size population within the quartz lens comprises a single girdle with activation of the prism
147 <a> and rhomb <a> slip systems (Fig. 4c). There is no indication of prism [c] activation. The
148 single girdle is inclined to the right, which is consistent with top-to-the-east-southeast shear.

149 The crystallographic fabric from the coarser grain-size population in the lens is similar to
150 that from the finer-sized population; activation of the prism <a> and rhomb <a> slip systems
151 dominates. Unlike the other intra-lens population, however, the fabric of the coarser-sized grains
152 forms a type-1 crossed-girdle (Fig. 4d). The main fabric displays a top-to-the-right (or southeast)
153 asymmetry, with secondary arms extending away from the main girdle (Fig. 4d).

154

155 *4.3 Quartz Crystallographic Fabric Interpretation*

156 With the exception of the prism [c] slip (discussed below) the fabric asymmetries noted
157 in the various specimen populations are consistent with interpreted top-to-the-east/southeast
158 movement across the nearby Tirich Mir and Reshun faults (Fig. 1; Calkins et al., 1981;
159 Hildebrand et al. 2001).

160 The quartz crystallographic fabric from the smaller grain-size population in the specimen
161 analysed indicates a component of prism [c] slip. Slip in the prism [c] direction is typically
162 associated with deformation in excess of 600 - 650 ˚C (Lister and Dornsiepen, 1982; Mainprice
163 et al., 1986; Morgan and Law, 2004). The rock sampled, however, is a low-metamorphic grade
164 phyllite and has not experienced temperatures in the range of those expected to favour prism [c]
165 slip.

166 Similar unexpected patterns have been noted in low-metamorphic grade slates and
167 phyllites in New Zealand where they are interpreted to reflect mechanical rotation of grains

168 elongate in the *c*-axis direction parallel with the stretching direction (Stallard and Shelly, 1995).
169 Such an interpretation is consistent with the sparse evidence of dynamic recrystallization in the
170 matrix quartz. However, *c*-axis orientations consistent with slip in the rhomb and prism <a>
171 directions indicate that there was some dynamic modification of the crystal lattice in response to
172 deformation. As suggested by Stallard and Shelly (1995), physical rotation of the clasts may
173 have occurred preferentially in the matrix grains surrounded by phyllosilicate-rich layers, into
174 which strain was preferentially partitioned. The matrix quartz grains that occur in areas with less
175 abundant phyllosilicate may have accommodated more of the strain directly through dislocation
176 slip resulting in the development of the prism <a> and rhomb/basal <a> *c*-axis orientations
177 observed in the crystallographic fabric.
178 The development of quartz *c*-axis maxima parallel to the stretching lineation may
179 alternatively be explained by preferential dissolution of quartz grains with their (0001) planes
180 parallel to the foliation. The dissolution of such grains and reprecipitation and/or concentration
181 of residual grains with *c*-axes parallel to the foliation have been interpreted to account for similar
182 *c*-axis patterns in low-metamorphic grade rocks in southeastern Brazil (Hippertt, 1994).
183 The orientations of *c*-axes in grains that comprise the quartz-rich lens in the specimen
184 appear to have been controlled by dynamic recrystallization (Fig. 3a-c) as part of their
185 deformational response to imposed stresses. Because the quartz records evidence of dynamic
186 recrystallization, the crystallographic fabrics measured from it are interpreted to reflect the
187 modification of its crystal lattice orientation in response to deformation.
188
189 *4.4 Deformation Temperature, Grain-Size Piezometry, and Strain Rate Estimates*
190 The crystallographic fabric from the coarser grains in the quartz lens forms a weakly
191 developed crossed-girdle fabric (Fig. 4d). The opening angle of such fabrics, that is the angle

between the arms of the fabric as measured about the perpendicular to the flow plane, have been empirically related to the estimated temperatures at which the fabrics developed (Kruhl, 1998; Morgan and Law, 2004; Law, 2014). Converting a fabric opening angle into a temperature of deformation requires a number of assumptions to be made, including temperature being the primary control on critically resolved shear stress, as opposed to strain rate or hydrolytic weakening. See Law (2014) for an in depth review of the considerations in using quartz crystallographic fabric opening angles as geothermometers. In reflection of the uncertainty in the data used for the empirical calibration and the precision of the opening angle determined, quartz crystallographic fabric-derived deformation temperatures are quoted at ± 50 ˚C (Kruhl, 1998).

The crossed girdle fabric in the specimen analysed has an opening angle of ~ 53 ˚ (Fig. 4d), which corresponds to a deformation temperature of ~ 403 ± 50 ˚C. That temperature estimate is consistent with the interpreted metamorphic grade of the rock and with the observed microstructures dominated by subgrain development with minor bulging. The transition from bulging to subgrain formation processes in the eastern Tonale fault zone of the Italian Alps is associated with temperatures near 400 ˚C (Fig. 9 of Stipp et al. 2002). Similar textures from the Himalaya may occur at slightly higher temperature, closer to 450 ˚C (Law, 2014). It should be noted, however, that, as with *c*-axis opening angles, strain rate and hydrolytic weakening can also play an important role in the development of quartz textures (e.g Law, 2014).

Recrystallized grain-size piezometry as proposed by Stipp and Tullis (2003) and recalibrated by Holyoke and Kronenburg (2010) may be used to estimate potential differences in differential flow stresses recorded in different dynamically recrystallized grain-size populations. Experimental calibration of the quartz grain-size piezometer applies to bulging recrystallization mechanisms and extends to a maximum grain-size of ~50 μm (Stipp and Tullis, 2003; Stipp et

al., 2006). Stipp et al. (2010) suggest that the piezometer may be reasonably applied to grains formed through subgrain rotation recrystallization, but would significantly underestimate those developed during grain boundary migration recrystallization. Applying the quartz recrystallization piezometer to the two dynamically recrystallized size populations in the quartz rich lenses yields differential stresses of 8.6 +2.6/-1.5 MPa and 15.0 +3.8/-2.5 MPa for the coarser and finer quartz grain-size populations respectively.

The differential stress estimates determined can be combined with deformation temperature and plotted atop a series of different geologically reasonable strain rates (Fig. 5). As pressure constraints have not been established for the specimen S32, or any relevant nearby locales, the fugacity used in both the Hirth et al., (2001) and Rutter and Brodie (2004) quartz flow law calibrations utilized was estimated using the derived deformation temperature, a thermal gradient of 25 ˚C/km, and an average crustal density of 2.85 g/cm^3. The resulting fugacity, 108 MPa, was calculated as in Pitzer and Sterner (1994). As noted in Law et al. (2013), calculated strain rates are rather insensitive to changes in fugacity; using a thermal gradient of 40 ˚C/km in fugacity calculations does not result in a significant change in the strain rate estimates for this study. Plotted differential stresses and deformation temperature indicates a faster strain rate for the finer grains/higher differential stress (Fig. 5). The strain rate estimates vary considerably between the two calibrations with only the Hirth et al. (2001) calibration providing estimates that approach those geologically reasonable (Fig. 5).

5. Discussion

The size variation between the matrix and lens quartz grains in the specimen may reflect primary differences associated with the protolith. The finer sized quartz grains found within the phyllitic matrix are interpreted to represent smaller grains deposited within a silt/mud-dominated

239 protolith, while the coarser quartz that occurs within the specimen is interpreted to represent a
240 thin sand lens. Within the lens itself the two grain size populations may reflect further primary
241 differences, secondary modification during deformation, or both. These possibilities are
242 discussed below.

243 It is possible that the two grain size populations within the lens reflect different strain
244 histories. The quartz within the lens has been subject to dynamic recrystallization during which
245 there would have been potential for the grains to change size and shape. The grain size difference
246 within the lens may reflect development of the finer population where stress was preferentially
247 partitioned resulting in more intense grain size reduction, whereas the courser population,
248 affected by lower stresses, may reflect more limited grain size reduction. Such stress partitioning
249 is consistent with differential stress estimates made based on grain size piezometry that indicated
250 higher stresses associated with smaller grain sizes.

251 The two grain sizes may, alternatively (or additionally), reflect an initial difference in
252 grain size inherited from the sand lens when it was first deposited, perhaps with compounded by
253 incomplete recrystallization of the larger grains. The variation in grain size within the quartz-
254 rich lens may represent a combination of both primary differences and secondary strain
255 partitioning. Finer grains within the quartz lens may have been preferred for initial strain
256 partitioning, which would have facilitated, and been enhanced by, further grain size reduction
257 and higher strain rates. Strain concentration within the finer grains in the quartz-rich lens is
258 consistent with the variation in crystallographic fabrics between the two size populations. The
259 coarser grain size fabric maintains secondary trailing arms (Fig 4d), whereas in the finer grain
260 size fabric those arms have been essentially obliterated (Fig. 4c). Migration towards a single
261 girdle fabric has been associated with increased critically resolved shear stress and shear strain

(Keller and Stipp, 2011) in quartz crystallographic fabric evolution models.

6. Conclusions

This study demonstrates the importance of spatial resolution and registration in specimens analyzed for crystallographic fabric analyses. In this metapelite example, the bulk crystallographic fabric overwhelmed two spatially restricted fabrics recorded in a quartz lens. Yet it was the secondary, spatially distinct fabrics that yielded information on deformation temperature, paleopiezometry, and strain rate. This has important implications for increasingly common studies that examine large numbers of specimens utilizing automated methods; care must be taken to investigate the spatial distribution of fabric symmetry within specimens as the bulk pattern may average and mask important information. The spatially-controlled crystallographic fabric patterns documented in this study may reflect the fundamental initial properties of the specimen, be products of differential strain partitioning at the microscale, or some combination of the two.

7. Acknowledgements

This project was supported by NSERC Discovery and CFI Leaders Opportunity Fund grants to K. Larson. A. Khan and the NCEG at the University of Peshawar are thanked for their logistical assistance during fieldwork. Discussions with D. Kellett, reviews by C. Wilson and , and editorial handling and review by R. Law have helped improve the clarity of the manuscript.

8. Fig. Captions

Fig. 1 - General geology map of the Garam Chasma/Chitral region, NW Pakistan (after Faisal et al., 2014). Specimen collection location is indicated. Field area location is shown in regional

286 scale inset map.

287

288 *Fig. 2* - Thin section scale photomicrographs of specimen S32 presented in plane-polarized light
289 (a), cross-polarized light (b), and as an AVA diagram (c). The location of quartz grains analysed
290 is indicated by different coloured and shaded circles in c. White circles denote a coarser grain
291 within the quartz-rich lens; black circles indicate a finer grain within a quartz-rich lens; yellow
292 circles mark a matrix quartz grain measured. A more detailed cross-polarized photomicrograph
293 of the quartz-rich lens is shown in d; coarser and finer populations are marked.

294

295 *Fig. 3* - Quartz microtextures observed in thin section. All photomicrographs are cross polarized
296 light. a) Three examples of minor bulging recrystallization. b) Subgrain development within the
297 quartz- rich lens. Also visible are deformation lamellae. c) Same location as in b) with the stage
298 rotated to further highlight subgrain formation. d) A matrix quartz grain (centre) encased by
299 phyllosilicates.

300

301 *Fig. 4* - Quartz crystallographic fabrics from various quartz populations in the specimen. All
302 diagrams are lower hemispherical equal area stereonet projections contoured at 1% intervals.
303 Contours for a) are 1, 2, 3, 4 times uniform; for b) through d) they are 1, 2, 3, 4, 5, 6+ times
304 uniform. The stereonets are oriented such that the foliation forms a vertical plane while the
305 observed lineation (and orientation of thin section) follows a horizontal E-W line. a)
306 Combined/bulk crystallographic fabric generated from an 8000-point grid mapped across the
307 specimen. b) Quartz crystallographic fabric generated from manually selected matrix grains. c)
308 Crystallographic fabric of the finer sized quartz population within the quartz-rich lens. d)
309 Crystallographic fabric of the coarser sized quartz population within the quartz-rich lens.

Fig. 5 - Strain rate estimates for the two size populations within the quartz rich lenses using the flow laws of Hirth et al. (2001) and Rutter and Brodie (2004). Differential stress estimates are from recrystallized grain-size piezometry while temperature estimates are from quartz crystallographic fabric opening angles. See text for discussion.

9. References

Blumenfeld, P., Mainprice, D. and Bouchez, J.-L.: *C*-slip in quartz from subsolidus deformed granite, Tectonophysics, 127, 97–115, 1986.

Bouchez, J.-L. and Pêcher, A.: Plasticite du quartz et sens de cisaillement dans des quartzites du Grand Chevaughement Central himalayen, Bulletin du societie geologique, France, 7(6), 1377–1385, 1976.

Calkins, J. A., Jamiluddin, S., Bhuyan, K. and Hussain, A.: Geology and Mineral Resources of the Chitral-Parstan Area, Hindu Kush Range, Northern Pakistan. Geological Survey (USA) Professional Paper 716-G, 1981.

Debon, F., Afzali, H., LeFort, P., Sonet, J.: Major intrusive stages in Afghanistan: typology, age, and geodynamic setting. Geologische Rundschau, 76(1), 245–264, 1987.

Desio, A.: On the geological age of some granites of the Karakoram, Hindu Kush and Badakhshan (central Asia). In: Proceeding of the 22nd International Geological Congress, Delhi, Part II, Section 11, 479–496, 1964.

Faisal, S., Larson, K. P., Cottle, J. M. and Lamming, J.: Building the Hindu Kush: Monazite Records of Terrane Accretion, Plutonism, and the Evolution of the Himalaya-Karakoram-Tibet Orogen, Terra Nova, n/a–n/a, doi:10.1111/ter.12112, 2014.

Gaetani, M., Le Fort, P., Tanoli, S., Angiolini, L., Nicora, A., Sciunnach, D. and Asif, K.:

Reconnaissance geology in Chitral, Baroghil and Karambar districts (N Pakistan). Geol Rundsch, 85, 683–704, 1996.

Heuberger, S., Schaltegger, U., Burgi, J.P., RG1, Villa, I.M., Frank, M., Dawood, H., Hussain, S., Zanchi, A.: Age and isotopic constraints on magmatism along the Karakoram-Kohistan Suture Zone, NW Pakistan: evidence for subduction and continued convergence after India-Asia collision. Swiss Journal of Geosciences, 100, 85–107, 2007.

Hildebrand, P. R., Noble, S. R., Searle, M. P., Parrish, R. R. and Shakirullah: Tectonic significance of 24 Ma crustal melting in the eastern Hindu Kush, Pakistan, Geology, 26(10), 871–874, 1998.

Hildebrand, P. R., Noble, S. R., Searle, M. P., Waters, D. J. and Parrish, R. R.: Old origin for an active mountain range: Geology and geochronology of the eastern Hindu Kush, Pakistan, Geol Soc Am Bull, 113(5), 625–639, 2001.

Hildebrand, P. R., Searle, M. P., Shakirullah, Khan, Z. and Van Heijst, H.: Geological evolution of the Hindu Kush, NW Frontier Pakistan: active margin to continent-continent collision zone, Geological Society London Special Publications, 170(1), 277–293, doi:10.1144/GSL.SP.2000.170.01.15, 2000.

Hippertt, J.F.: Microstructures and *c*-axis fabrics indicative of quartz dissolution in sheared quartzites and phyllonites, Tectonophysics, 229, 141-163, 1994.

Hirth, G. and Tullis, J.: Dislocation creep regimes in quartz aggregates, Journal of Structural Geology, 14, 145–160, 1992.

Hirth, G., Teyssier, C. and Dunlap, J.: An evaluation of quartzite flow laws based on comparisons between experimentally and naturally deformed rocks, International Journal of Earth Sciences, 90(1), 77–87, doi:10.1007/s005310000152, 2001.

Holyoke, C. W., III and Kronenberg, A. K.: Accurate differential stress measurement using the molten salt cell and solid salt assemblies in the Griggs apparatus with applications to strength, piezometers and rheology, Tectonophysics, 494(1-2), 17–31, doi:10.1016/j.tecto.2010.08.001, 2010.

Keller, L. M. and Stipp, M.: The single-slip hypothesis revisited: Crystal-preferred orientations of sheared quartz aggregates with increasing strain in nature and numerical simulation, Journal of Structural Geology, 33(10), 1491–1500, doi:10.1016/j.jsg.2011.07.008, 2011.

Kile, D.E.: The universal stage: The past, present, and future of a mineralogical research instrument. Geochemical News, 140, 2009.

Kruhl, J. H.: Reply: Prism- and basal plane parallel subgrain boundaries in quartz: a microstructural geothermobarometer, Journal of Metamorphic Geology, 16, 142–146, 1998.

Larson, K. P. and Cottle, J. M.: Midcrustal discontinuities and the assembly of the Himalayan midcrust, Tectonics, doi:10.1002/(ISSN)1944-9194, 2014.

Law, R. D., Schmid, S. and Wheeler, J.: Simple Shear Deformation and Quartz Crystallographic Fabrics - a Possible Natural Example From the Torridon Area of Nw Scotland, Journal of Structural Geology, 12(1), 29–45, 1990.

Law, R.D., Deformation thermometry based on quartz *c*-axis fabrics and recrystallization microstructures: A review, Journal of Structural Geology, 66, 129-161, 2014

Law, R. D., Searle, M. P. and Simpson, R. L.: Strain, deformation temperatures and vorticity of flow at the top of the Greater Himalayan Slab, Everest Massif, Tibet, Journal of the Geological Society, 161, 305–320, 2004.

Law, R. D., Mainprice, D., Casey, M., Lloyd, G., Knipe, R., Cook, B. and Thigpen, J.: Moine

Thrust zone mylonites at the Stack of Glencoul: I-microstructures, strain and influence of recrystallization on quartz crystal fabric development, Geological Society London Special Publications, 335(1), 543, 2010.

Law, R. D., Jessup, M. J., Searle, M. P., Francsis, M. K., Waters, D. J. and Cottle, J. M.: Telescoping of isotherms beneath the South Tibetan Detachment System, Mount Everest Massif, Journal of Structural Geology, 1–26, doi:10.1016/j.jsg.2011.09.004, 2011.

Law, R. D., Stahr, D. W., Francsis, M. K., Ashley, K. T., Grasemann, B. and Ahmad, T.: Deformation temperatures and flow vorticities near the base of the Greater Himalayan Series, Sutlej Valley and Shimla Klippe, NW India, Journal of Structural Geology, 1–93, doi:10.1016/j.jsg.2013.05.009, 2013.

Lister, G. S. and Dornsiepen, U. F.: Fabric transitions in the Saxony granulite terrain, Journal of Structural Geology, 4, 81–92, 1982.

Lister, G. S. and Williams, P. F.: Fabric development in shear zones: theoretical controls and observed phenomena, Journal of Structural Geology, 1(4), 283–297, 1979.

Mainprice, D. Bouchez, J.L., Blumenfeld, P., and Tubia, J.M: Dominant *c* slip in naturally deformed quartz: implications for dramatic plastic softening at high temperature, Geology, 14, 819-822, 1986.

Morgan, S.S. and Law, R.D.: Unusual transition in quartzite dislocation creep regimes and crystal slip systems in the aureole of the Eureka Valley-Joshua Flat-Beer Creek pluton, California: a case for anhydrous conditions created by decarbonation reactions, Tectonophysics, 384, 209-231, 2004.

Peternell, M., Hasalová, P., Wilson, C. J. L., Piazolo, S. and Schulmann, K.: Evaluating quartz crystallographic preferred orientations and the role of deformation partitioning using

403 EBSD and fabric analyser techniques, Journal of Structural Geology, 32(6), 803–817,
404 doi:10.1016/j.jsg.2010.05.007, 2010.
405 Pitzer, K.S. and Sterner, S. M.: Equations of state valid continuously from zero to extreme
406 pressures for H20 and CO2, The Journal of Chemical Physics, 101, 3111-3116, 1994.
407 Prior, D. J., Boyle, A. P., Brenker, F., Cheadle, M. C., Day, A., Lopez, G., Peruzzo, L., Potts, G.
408 J., Reddy, S., Speiss, R., Timms, N. E., Trimby, P., Wheeler, J. and Zetterström, L.: The
409 application of electron backscatter diffraction and orientation contrast imaging in the
410 SEM to textural problems in rocks, American Mineralogist, 84, 1741-1759, 1999.
411 Rutter, E. and Brodie, K.: Experimental intracrystalline plastic flow in hot-pressed synthetic
412 quartzite prepared from Brazilian quartz crystals, Journal of Structural Geology, 26, 259–
413 270, 2004.
414 Sander, B.: Einführung in die Gefügekunde der Geologischen Körper, Zweiter Teil, Die
415 Korngefuege, Springer-Verlag, Wein-Inssbruck, 1950.
416 Schmid, S.M. and Casey, M.: Complete fabric analysis of some commonly observed quartz [c]-
417 axis patterns. In: Hobbs, B.E., Heard, H.C. (Eds.), Mineral and Rock Deformation:
418 Laboratory Studies. Geophysical Monograph 36, 263-286, 1986.
419 Stallard, A. and Shelly, D.: Quartz c-axes parallel to stretching directions in very low-grade
420 metamorphic rocks, Tectonophysics, 249, 31-40, 1995.
421 Stipp, M. and Tullis, J.: The recrystallized grain size piezometer for quartz, Geophys Res Lett,
422 30(21), doi:10.1029/2003GL018444, 2003.
423 Stipp, M., Stünitz, H., Heilbronner, R., and Schmid, S.M.: The eastern Tonale fault zone: a
424 natural laboratory for crystal plastic deformation of quartz over a temperature range from
425 250 to 700° C, Journal of Structural Geology, 24, 1861-1884, 2002.

426 Stipp, M., Tullis, J. and Behrens, H.: Effect of water on the dislocation creep microstructure and
427 flow stress of quartz and implications for the recrystallized grain size piezometer, Journal
428 of Geophysical Research, 111, B042201, http://dx.doi.org/10.1029/2005JB003852, 2006.
429 Stipp, M., Tullis, J., Scherwath, M. and Behrmann, J. H.: A new perspective on paleopiezometry:
430 Dynamically recrystallized grain size distributions indicate mechanism changes,
431 Geology, 38(8), 759–762, doi:10.1130/G31162.1, 2010.
432 Turner, F.J.: Preferred orientation of olivine crystals in peridotite, Transactions and Proceedings
433 of the Royal Society of New Zealand, 72, 280-300, 1942
434 Wenk, H. –R. (Editor): Preferred Orientaiton in Deformed Metals and Rocks: An introduction to
435 Modern Texture Analysis. Academic Press, London, 610 p., 1985.
436 Wilson, C. J. L., Russell-Head, D. S., and Sim, H. M.: The application of an automated fabric
437 analyser system to the textural evolution of folded ice layers in shear zones. Annals
438 Glaciology, 37, 7-17, 2003.
439 Wilson, C. J. L., Russell-Head, D. S., Kunze and Viola, G.: The analysis of quartz c-axis fabrics
440 using a modified optical microscope, Journal of Microscopy, 227, 30–41, 2007.
441 Wilson, C. J. L., Robinson, J. and Dugdale, A.: Quartz vein fabrics coupled to elevated fluid
442 pressures in the Stawell gold deposit, south-eastern Australia, Mineralium Deposita,
443 44(3), 245–263, 2009.
444 Wilson, C. J. L. and Peternell, M. A.: Evaluating ice fabrics using fabric analyser techniques in
445 Sørsdal Glacier, East Antarctica, Journal of Glaciology, 57, 881-894, 2011.
446 Xypolias, P. and Koukouvelas, I. K.: Kinematic vorticity and strain rate patterns associated with
447 ductile extrusion in the Chelmos Shear Zone (External Hellenides, Greece),
448 Tectonophysics, 338(1), 59–77, doi:10.1016/S0040-1951(01)00125-1, 2001.

Zanchi, A. and Gaetani, M.: The geology of the Karakoram range, Pakistan: the new 1:100,000 geological map of Central-Western Karakoram. Italian Journal of Geosciences, 130, 161–262, 2011.

Zanchi, A., Poli, S., Fumagalli, P. and Gaetani, M.: Mantle exhumation along the Tirich Mir Fault Zone, NW Pakistan: pre-mid-Cretaceous accretion of the Karakoram terrane to the Asian margin. In: Tectonics of the Nanga Parbat Syntaxis and the Western Himalaya (M.A. Khan, P.J. Treloar, M.P. Searle and M.Q. Jan, eds). Geological Society of London, Special. Publication, 170, 237–252, 2000.

Zhang, S. and Karato, S.I.: Lattice preferred orientation of olivine aggregates deformed in simple shear, Nature, 375, 774-777, 1995.

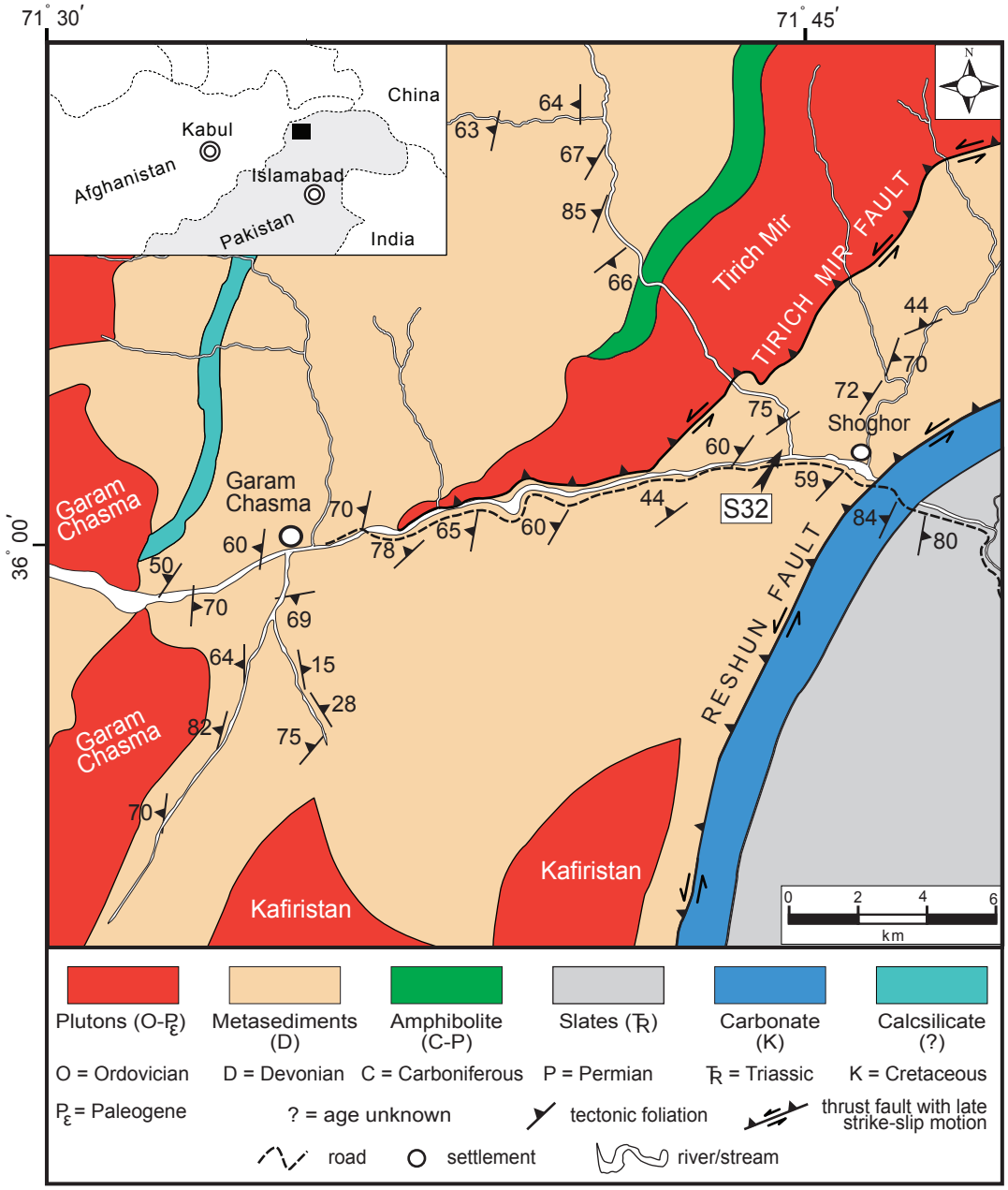
71° 30′
71° 45′
36° 00′
China
Kabul
Afghanistan
Islamabad
Pakistan
India
N
Tirich Mir
TIRICH MIR FAULT
Garam Chasma
Garam Chasma
Garam Chasma
Shoghor
S32
RESHUN FAULT
Kafiristan
Kafiristan
0 2 4 6
km
Plutons (O-Pε)
Metasediments (D)
Amphibolite (C-P)
Slates (TR)
Carbonate (K)
Calcsilicate (?)
O = Ordovician
D = Devonian
C = Carboniferous
P = Permian
TR = Triassic
K = Cretaceous
Pε = Paleogene
? = age unknown
tectonic foliation
thrust fault with late strike-slip motion
road
settlement
river/stream

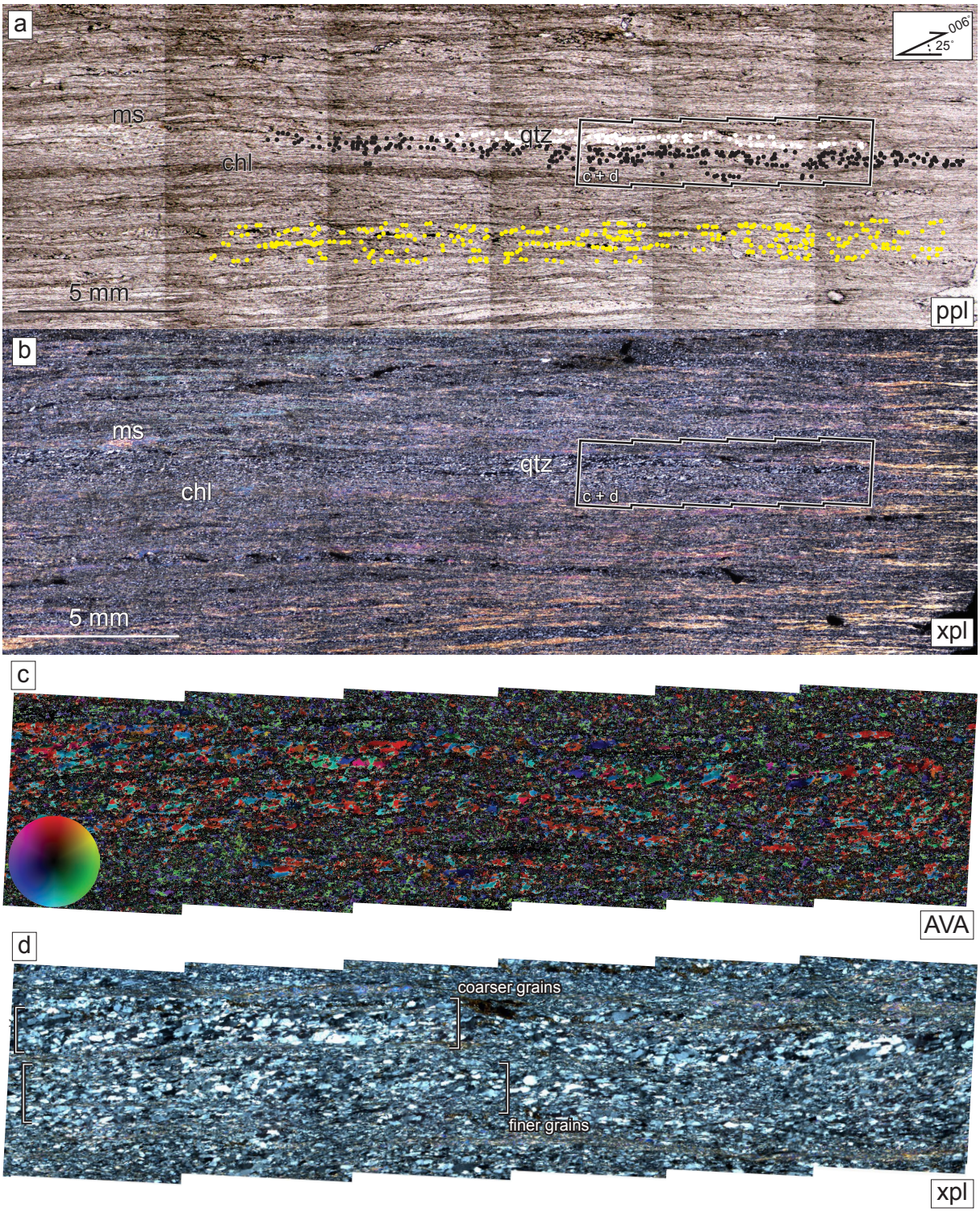
a
ms
chl
qtz
c + d
5 mm
ppl
b
ms
chl
qtz
c + d
5 mm
xpl
c
AVA
d
coarser grains
finer grains
xpl

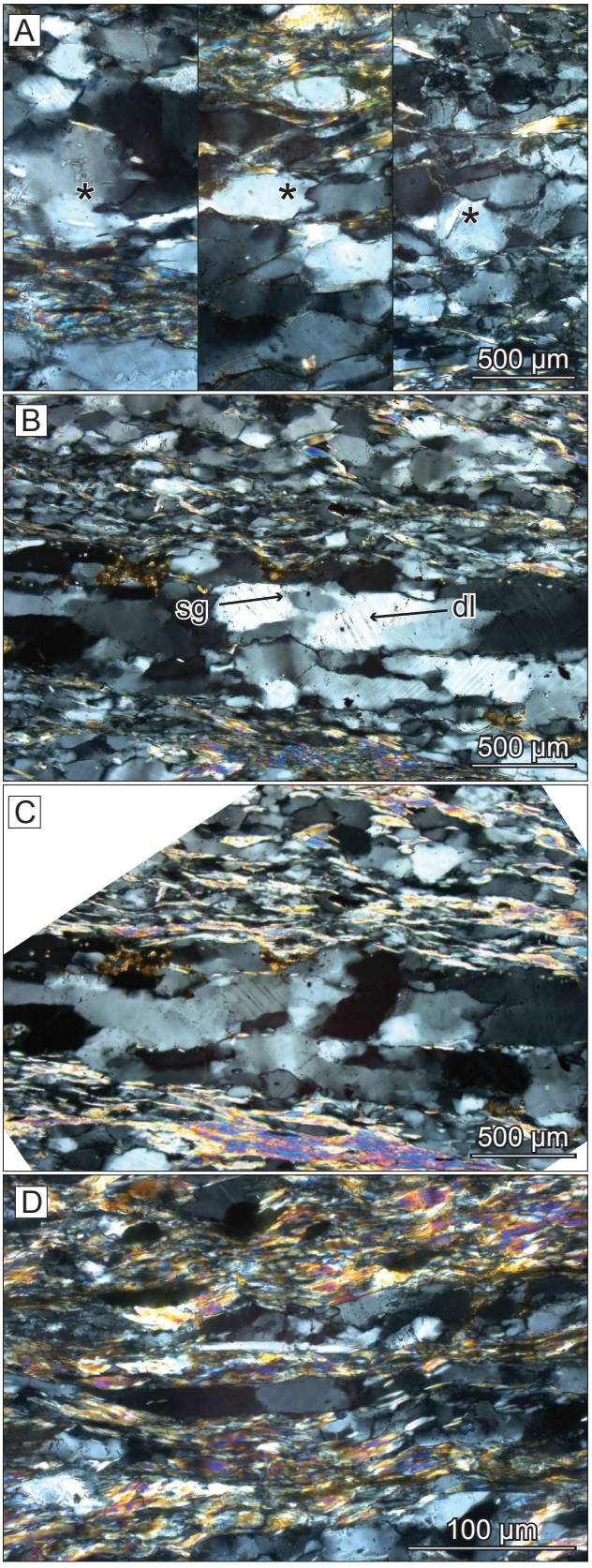
A
*
*
*
500 µm
B
sg
dl
500 µm
C
500 µm
D
100 µm

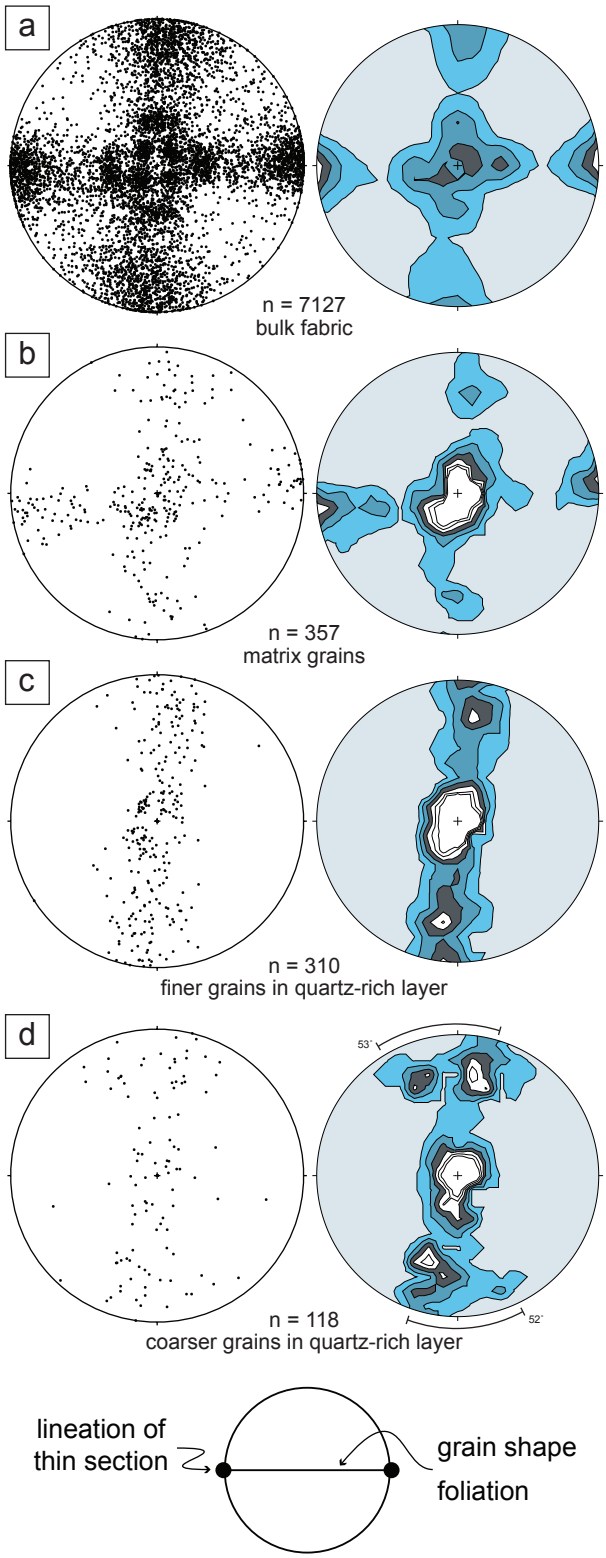

Thin section was cut along a line
equivalent to a lineation of
25˚ → 006˚

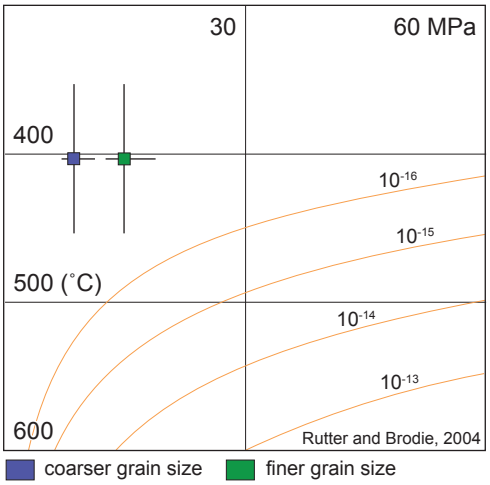
30
60 MPa
400
500 (˚C)
600
10-16
10-15
10-14
10-13
Rutter and Brodie, 2004
coarser grain size
finer grain size

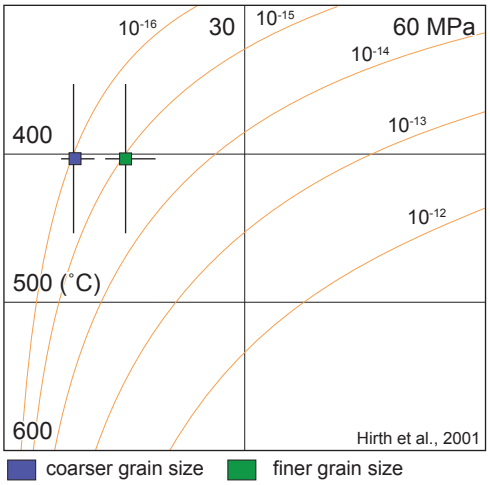
10-16
30
10-15
60 MPa
10-14
400
10-13
500 (˚C)
10-12
600
Hirth et al., 2001
coarser grain size
finer grain size